第三十九届中国控制会议

The 39th Chinese Control Conference

程序册

Final Program

主办单位

中国自动化学会控制理论专业委员会

中国自动化学会

中国系统工程学会

承办单位

东北大学

Sponsoring Organizations

Technical Committee on Control Theory, Chinese Association of Automation

Chinese Association of Automation

Systems Engineering Society of China

Northeastern University, China

2020 年 7 月 27-29 日，中国 • 沈阳

July 27-29, 2020, Shenyang, China

Mao, Nannan — Dalian Maritime Univ.

WeA10 13:30–15:50
Regular Session: Navigation and Guidance (3)

Chair: Zou, Yiqun — Central South Univ.
Co-Chair: Guo, Yanbing — China Electronics Tech. Group Corporation

▶ WeA10-1 13:30–13:50
1549 *Micro Aerial Vehicle Yaw Estimation and Localization Based on Ultrasonic Sensors in Indoor Environment*
Xu, Jiwen — Beihang Univ.
Yang, Lingyu — Beihang Univ.
Xu, Jiang Peng — Beihang Univ.
Feng, Xiaoke — Beihang Univ.
Zhang, Jing — Beihang Univ.

▶ WeA10-2 13:50–14:10
1590 *Angles-Only Relative Navigation in Spherical Coordinates Using Unscented Kalman Filter*
Han, Fei — Shanghai Aerospace Control Tech. Research Inst.
Wang, Zhaolong — Shanghai Key Laboratory of Aerospace Intelligence Control Tech.
Han, Yu — Shanghai Inst. of Spaceflight Control Tech.
Liu, Chaozhen — CASC

▶ WeA10-3 14:10–14:30
1709 *An Instrumental-variable Method for Bearing-only Localization under Small Noise*
Zou, Yiqun — Central South Univ.
Gao, Bilu — Central South Univ.
Tang, Xiafei — Changsha Univ. of Sci. & Tech.
Yu, Lingli — Central South Univ.

▶ WeA10-4 14:30–14:50
2084 *Geomagnetic Perceiving Navigation Method for Autonomous Underwater Vehicle Using An Adapted Search Strategy*
Li, Hong — Xi'an Univ. of Posts & Telecommunications

▶ WeA10-5 14:50–15:10
2162 *Regional Geomagnetic Map Construction Based on Support Vector Machine Residual Kriging*
Liu, Tong — Beijing Inst. of Tech.
Li, Xingyu — Beijing Inst. of Tech.
Fu, Mengyin — Beijing Inst. of Tech.
Liang, Zhaoxiang — Beijing Inst. of Tech.

▶ WeA10-6 15:10–15:30
2242 *Maximum Correntropy Criterion Kalman Filter Based Target Tracking with State Constraints*
Zou, Yiqun — Central South Univ.
Zou, Shuang — School of Automation, Central South Univ.
Tang, Xiafei — Changsha Univ. of Sci. & Tech.
Yu, Lingli — Central South Univ.

▶ WeA10-7 15:30–15:50
2384 *The Optimized Design of the Navigation Filter*
Guo, Yanbing — China Electronics Tech. Group Corporation
Miao, Ling-Juan — Beijing Inst. of Tech.,
Zhang, Xi — Qianxun SI Inc

WeA11 13:30–15:30
Regular Session: Fault Diagnosis and Reliable Control (3)

Chair: Yang, Hao — Nanjing Univ. of Aeronautics & Astronautics
Co-Chair: Cui, Jianguo — Shenyang Aerospace Univ.

▶ WeA11-1 13:30–13:50
1740 *Gaussian Mixture Model Based Fault Diagnosis for Elevator Overspeed and Automatic Reset*
Zheng, Qi — College of Control Sci. & Engineering, Zhejiang Univ.
Zhao, Chunhui — Zhejiang Univ.

▶ WeA11-2 13:50–14:10
1749 *Anomaly Detection and Remaining Useful Life Estimation Based on Degradation State for Bearings*
Hu, Xiangzhi — Shanghai Jiao Tong Univ.
Li, Ning — Shanghai Jiao Tong Univ.

▶ WeA11-3 14:10–14:30
1962 *Fault Tolerant Control of Centralized Potential Games*
Lu, Shi — Nanjing Univ. of Aeronautics & Astronautics
Yang, Hao — Nanjing Univ. of Aeronautics & Astronautics
Jiang, Bin — Nanjing Univ. of Aeronautics & Astronautics

▶ WeA11-4 14:30–14:50
1964 *Fault Tolerant Control for A Class of Evolutionary Matrix Games*
Ni, Yuan — Nanjing Univ. of Aeronautics & Astronautics
Yang, Hao — Nanjing Univ. of Aeronautics & Astronautics
Jiang, Bin — Nanjing Univ. of Aeronautics & Astronautics

▶ WeA11-5 14:50–15:10
1990 *A Method for Fault Diagnosis of Aviation Engine Gas System*
Cui, Jianguo — Shenyang Aerospace Univ.
Tian, Yan — Shenyang Aerospace Univ.
Cui, Xiao — Shenyang Aerodynamics Research Inst.
Wang, Jinglin — Aviation Key Laboratory of Sci. & Tech. on Fault Diagnosis & Health Management
Jiang, Liying — Shenyang Aerospace Univ.
Yu, Mingyue — Automatization Engineering Collede Shenyang Aerospace Univ. LiaoNing Province

▶ WeA11-6 15:10–15:30
2218 *Fault-tolerant Control for Multi-agent with Actuator Fault*
Zhang, Pu — Northwestern Polytechnical Univ.
Xue, Huifeng — Northwestern Polytechnical Univ.
Gao, Shan — Northwestern Polytechnical Univ.

WeA12 13:30–15:50
Regular Session: Social/Economic Systems and Control

Chair: Xu, Yaoqun — Harbin Univ. of Commerce
Co-Chair: Tie, Lin — Beihang Univ. (Beijing Univ. of Aeronautics & Astronautics)

▶ WeA12-1 13:30–13:50
1659 *Supply Chain Coordination of Consumer Electronics Products Considering Product Quality Level*
Xu, Yaoqun — Harbin Univ. of Commerce
Yu, Qijia — Harbin Univ. of Commerce
Zheng, Yi — Harbin Univ. of Commerce

▶ WeA12-2 13:50–14:10
1851 *Stock Price Volatility, Equity Balance and Corporate M&A*
Zhu, Guanping — Xi´an Univ. of Tech.
Hu, Wenxiu — Xi'an Univ. of Tech.
Che, Shanshan — Xi'an Univ. of Tech.
Yang, Dong — People's Insurance Company of China

▶ WeA12-3 14:10–14:30
2086 *Research on CDS Spread of Credit Bonds in China Based on Vasicek Model*
Yang, Ruicheng — Inner Mongolia Univ. of Finance & Economics
You, Wei — Inner Mongolia Univ. of Finance & Economics
Wang, Xuetao — Inner Mongolia Univ. of Finance & Economics

▶ WeA12-4 14:30–14:50
2370 *Optimization Model for Safety Investment of Prefabricated Building Construction*
Chang, Chun Guang — Shenyang Jianzhu Univ.
Zhao, Teng — Shenyang Jianzhu Univ.

▶ WeA12-5 14:50–15:10
2476 *The Applicability of SIMM in the Chinese Options Market Compared to SPAN*
Shi, Ruoshi — Chinese Acad. of Sci.
Zhao, Yanlong — Chinese Acad. of Sci.

▶ WeA12-6 15:10–15:30
0035 *Based on "Automatic Control Theory Experiment" MOOC+SPOC Teaching Management*
Jiang, Zengru — Beijing Inst. of Tech.
Jin, Honglong — Beijing Inst. of Tech.

▶ WeA12-7 15:30–15:50
1865 *Improvement for Root Locus Method Teaching by Introducing New Applications*
Tie, Lin — Beihang Univ. (Beijing Univ. of Aeronautics & Astronautics)

WeA13 13:30–15:30
Regular Session: Multi-Agent Systems and Distributed Control (5)

Chair: Lu, Shaobo — Chongqing Univ.
Co-Chair: Sun, Xinmiao — Univ. of Sci. & Tech. Beijing

▶ WeA13-1 13:30–13:50
2373 *Optimal Coverage Control of Multi-agent Systems in Constrained Environments with Line-of-sight Connectivity Preservation*

Proceedings of the 39th Chinese Control Conference
July 27-29, 2020, Shenyang, China

Micro Aerial Vehicle Yaw Estimation and Localization Based on Ultrasonic Sensors in Indoor Environment

Jiwen Xu[1], Lingyu Yang[1,*], Jiangpeng Xu[1], Xiaoke Feng[1,2], Jing Zhang[1]

1. School of Automation Science and Electrical Engineering, Beihang University, Beijing 100191, China
*Corresponding author, E-mail: yanglingyu@buaa.edu.cn

2. AVIC Chengdu Aircraft Design & Research Institute, Chengdu 610091, China

Abstract: This paper addresses the problem of yaw angle estimation and indoor positioning of micro aerial vehicle (MAV) under GPS-free environment and complex electromagnetic interference. A distance-ranging-based approach is proposed to localize MAV. The relation of ultrasonic sensors measurements and MAV position as well as yaw angle is given by establishing a nonlinear, implicit, and piecewise continuous model. Thus, the extended Kalman filter (EKF) is applied to estimate the MAV position and yaw angle according to ultrasonic sensors and inertial measurement unit. Furthermore, a jump filter is introduced to compensate the mutation caused by discontinuity of the model. Simulations are presented and the results show the effectiveness of the algorithm.

Key Words: MAV yaw estimation, indoor localization, EKF algorithm

1 Introduction

In recent years, micro aerial vehicles (MAV) attitude estimation and positioning technology have been broadly concerned in numerous fields as a basic technical support for MAV to accomplish complicated tasks, such as ultra-low altitude reconnaissance and surveillance[1][2]. Due to the characteristics of low-cost, small-size, and high mobility, it is also possible to enter places with safety hazards to help detect interior conditions of large buildings and facilities in place of manpower[3][4]. However, multiple magnetic interference factors in complex indoor environment also make it impossible for MAV to use magnetic compass for accurate orientation[5][6], and decreased GPS positioning accuracy due to blocking and multi-path effect between buildings requires additional sensors to accomplish localization [7].

Based on raised problems, additional information is needed to improve the yaw angle estimation accuracy. Hardware redundancy and analytical redundancy are two types of improvement[8]. The former indicates multiple sensor system providing additional information to estimate the yaw angle, which is difficult to achieve within MAV payload limits. The analytical redundancy is designed based on model characteristics, where visual information is often incorporated into the estimator, decreasing the instability brought by the electromagnetic interference. [9] proposed an optical flow sensor model/inertial measurement unit (IMU) fault-tolerant fusion to achieve yaw angle estimation, which is also a strict demand for MAV loading capacity.

Current positioning technology mainly adopts vision-based and multi sensor-based positioning methods. The former approach mostly requires optical motion capture system or cameras. In [10], an optical flow algorithm was applied to determine the position and direction of MAV by calculating the image gradient of the robot vision scene. [11] utilized a monocular visual simultaneous localization and mapping (SLAM) system consisted of two cameras to complete localization mission. But in a complex indoor condition, large amount of calculation of SLAM may cause time delay in control system. According to [12], MAV achieved relatively stable positioning by communicating with mobile ground vehicles through ultra wide band (UWB). Other positioning methods based on distance sensors[13], visual sensor[14], ZigBee[15] , etc. are equally capable to impair external disturbance and modify estimation error of IMU. Multi sensor-based approaches rely on either on-board sensors or ground-based facilities, which cannot be utilized universally due to the environment complexity.

In this paper, an extended Kalman filter (EKF) based on range measurement is presented to improve MAV yaw angle estimation and localization performance. The framework is as follows. The second section introduces MAV indoor positioning system model, while the yaw estimation, localization, and EKF information fusing process are displayed in the third section. In the fourth section, simulation results are demonstrated to verify the reliability of the algorithm.

2 System Model

The MAV platform structure is demonstrated as Fig. 1, which technical details are explained in [1]. Four SRF01 ranging sensors are mounted perpendicularly to each other at the bottom of the MAV, thus the sensor system can provide ranges of four directions in a single measurement.

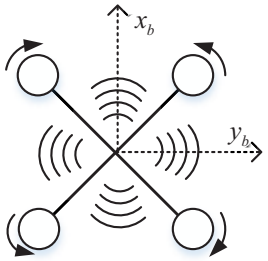

Fig. 1：The sketch of MAV

Two coordinate systems are established in this paper. The map coordinate system $O-x_m y_m z_m$ and the body coordinate system $O-x_b y_b z_b$ are shown in Fig. 2. $\boldsymbol{m}_i$ represents coordinates of infection points of prior map, therefore the transcendental environment can be described as a set of walls represented by a set of line segments $\mathcal{M}=\{\boldsymbol{M}_1,\boldsymbol{M}_2,...,\boldsymbol{M}_n\}$, where $\boldsymbol{M}_i$ denotes a line segment with endpoints $\boldsymbol{m}_i$ and $\boldsymbol{m}_{i+1}$ as

$$\boldsymbol{M}_i=\overline{\boldsymbol{m}_i\boldsymbol{m}_{i+1}}, i=1,2,...,n-1 \tag{1}$$

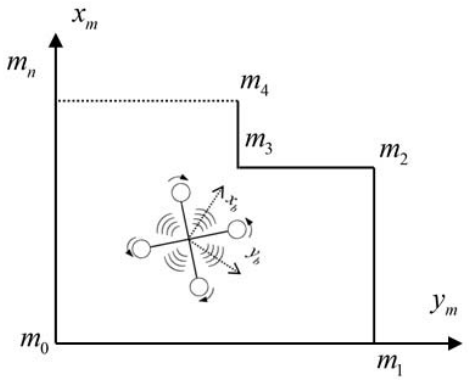

Fig. 2：Map coordinate system and body coordinate system

The yaw angle of the MAV in the map coordinate system is marked as ψ, which is positive for clockwise rotation. The rotation matrix between body frame and map frame is

$$\boldsymbol{R}_{mb}=\begin{bmatrix}\cos\psi & -\sin\psi\\ \sin\psi & \cos\psi\end{bmatrix} \tag{2}$$

The acceleration of the MAV in two frames are derived as

$$\boldsymbol{a}_m=\boldsymbol{R}_{mb}\cdot\boldsymbol{a}_b \tag{3}$$

where $\boldsymbol{a}_b$ represents acceleration of MAV in body coordinate system, while $\boldsymbol{a}_m$ represents acceleration in map coordinate system. Define (x_M,y_M) as the position of MAV in the prior map, v_x,v_y as MAV velocity in x_m and y_m direction, and a_x,a_y are MAV accelerated speed along x_b and y_b in the body coordinate system. Suppose that MAV works at a fixed altitude, and T_A represents the sampling interval of IMU sensors, thus the MAV model is formed as (4).

$$\begin{cases}x_M(k+1)=x_M(k)+v_x(k)T_A+\frac{1}{2}[a_x(k)\cos\psi(k)\\ \qquad -a_y(k)\sin\psi(k)]T_A^{\,2}+w_1(k)\\ v_x(k+1)=v_x(k)+[a_x(k)\cos\psi(k)-a_y(k)\sin\psi(k)]T_A+w_2(k)\\ y_M(k+1)=y_M(k)+v_y(k)T_A+\frac{1}{2}[a_x(k)\sin\psi(k)\\ \qquad +a_y(k)\cos\psi(k)]T_A^{\,2}+w_3(k)\\ v_y(k+1)=v_y(k)+[a_x(k)\sin\psi(k)+a_y(k)\cos\psi(k)]T_A+w_4(k)\\ \psi(k+1)=\psi(k)+\omega_z T_A+w_5(k)\end{cases} \tag{4}$$

MAV model with noise disturbance can be briefly described as

$$\boldsymbol{x}(k+1)=\boldsymbol{f}\left(\boldsymbol{x}(k),\boldsymbol{u}(k)\right)+\boldsymbol{w}(k) \tag{5}$$

$\boldsymbol{w}(k)=[w_1(k),w_2(k),w_3(k),w_4(k),w_5(k)]^T$ represents white noise with a mean of zero and a variance of $\boldsymbol{Q}$, and $\boldsymbol{u}(k)=\left[a_x(k),a_y(k),\omega_z(k)\right]^T$ is the control input of the MAV system.

The estimated values in four directions $\boldsymbol{l}=(l_1,l_2,l_3,l_4)^T$ acquired by SRF01 sensors are considered in MAV observation equations. SRF01 sonar beam is modeled as in Fig. 3.

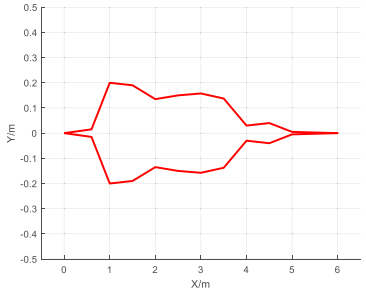

Fig. 3：The beam pattern of SRF01 sonic sensor

On account of the complexity of on-line calculation of the sensor beam model, a simplified multi-ray ultrasonic model is purposed according to the experiment results in [1] as Fig. 4.

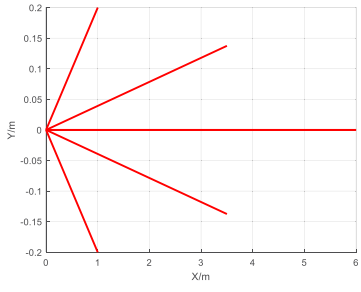

Fig. 4：Multi-ray sonar model

Thus the ultrasonic 2D multi-ray model S can be formulated as a ray group where

$$\begin{cases}S=\{\boldsymbol{S}_1,\boldsymbol{S}_2,...,\boldsymbol{S}_k\}\\ \boldsymbol{S}_1=\overline{\boldsymbol{s}_0\boldsymbol{s}_1},\boldsymbol{S}_2=\overline{\boldsymbol{s}_0\boldsymbol{s}_2},...,\boldsymbol{S}_k=\overline{\boldsymbol{s}_0\boldsymbol{s}_k}\end{cases} \tag{6}$$

S can be described as a set of rays $\boldsymbol{S}_k$, and $\boldsymbol{s}_0, \boldsymbol{s}_1, \ldots, \boldsymbol{s}_k$ represent the endpoints of rays respectively. The intersecting points of S and $\mathcal{M}$ are formed as $\mathcal{R}$, where

$$\mathcal{R} = S \otimes \mathcal{M} = \{\boldsymbol{r}_1, \boldsymbol{r}_2, \ldots \boldsymbol{r}_q\} \tag{7}$$

The minimum l is selected as the estimated value of the ultrasonic sensor as in (8).

$$l = \begin{cases} \min\limits_{\boldsymbol{r}_i} \|\boldsymbol{r}_i - \boldsymbol{s}_0\|_2, & \mathcal{R} \neq \varnothing \\ l_{\max}, & \mathcal{R} = \varnothing \end{cases} \quad i = 1,2,\ldots,q \tag{8}$$

According to [1], among all intersections, the one that minimizes (8) is defined as the "active intersection" $\boldsymbol{r}_a$, and terms "active ray" $\boldsymbol{S}_a$ and "active wall" $\boldsymbol{M}_a$ are introduced to represent the corresponding ray and the corresponding wall with the active intersection. Hence the observation equation can be described as

$$\boldsymbol{l}(k) = \boldsymbol{h}(x_M(k), y_M(k), \psi(k), \mathcal{M}, S) + \boldsymbol{v}(k) \tag{9}$$

$\boldsymbol{v}(k) = [v_1(k), v_2(k), v_3(k)]^T$ represents white measurement noise with a mean of zero and a variance of $\boldsymbol{R}$.

Remark 1: It is noted that $\boldsymbol{l}$ is a function of x_M, y_M and ψ, thus the above state variables can be estimated through $\boldsymbol{l}$ respectively. However, due to its nonlinearities and implicitness, $\boldsymbol{l}(k)$ cannot be estimated directly during filtering procedure, therefore a fast algorithm is presented in section 3 to carry out the estimation.

Remark 2: Due to the fact that during the estimation process, $\boldsymbol{M}_a$ in the prior map will switch from one to another, distances calculated by the multi-ray model may mutate because of the switch. Therefore $\boldsymbol{h}(\cdot)$ is characterized by piecewise continuity, which leads to difficulties in the estimation of $\boldsymbol{l}(k)$.

3 Estimation Algorithm

3.1 Linearization Results

The discrete nonlinear model of the MAV is given as

$$\begin{cases} \boldsymbol{x}(k+1) = \boldsymbol{f}(\boldsymbol{x}(k), \boldsymbol{u}(k)) + \boldsymbol{w}(k) \\ \boldsymbol{l}(k+1) = \boldsymbol{h}(\boldsymbol{x}(k+1), \mathcal{M}, S) + \boldsymbol{v}(k+1) \end{cases} \tag{10}$$

Because of the nonlinearity of (10), linearizing approach is utilized to carry out approximation. Define $\hat{\boldsymbol{x}}(k|k)$ as the estimated value of state variables at previous time k, $\hat{\boldsymbol{x}}(k+1|k)$ as the predicted value calculated from (4) based on $\hat{\boldsymbol{x}}(k|k)$. Taylor formula is applied in $\boldsymbol{f}(\cdot)$ at $\hat{\boldsymbol{x}}(k|k)$ and $\boldsymbol{h}(\cdot)$ at $\hat{\boldsymbol{x}}(k+1|k)$ to obtain (11) and (12).

$$\boldsymbol{x}(k+1) = \boldsymbol{f}(\hat{\boldsymbol{x}}(k|k), \boldsymbol{u}) + \frac{\partial \boldsymbol{f}}{\partial \boldsymbol{x}(k)}\Big|_{\hat{\boldsymbol{x}}(k|k)} (\boldsymbol{x}(k) - \hat{\boldsymbol{x}}(k|k)) + \boldsymbol{w}(k) \tag{11}$$

$$\boldsymbol{l}(k+1) = \boldsymbol{h}(\hat{\boldsymbol{x}}(k+1|k)) + \frac{\partial \boldsymbol{h}}{\partial \boldsymbol{x}(k)}\Big|_{\hat{\boldsymbol{x}}(k+1|k)} (\boldsymbol{x}(k+1) - \hat{\boldsymbol{x}}(k+1|k)) + \boldsymbol{v}(k+1) \tag{12}$$

$\boldsymbol{\Phi}(k+1|k), \boldsymbol{H}(k), \boldsymbol{p}(k)$ are defined as

$$\boldsymbol{\Phi}(k+1|k) = \frac{\partial \boldsymbol{f}}{\partial \boldsymbol{x}(k)}\Big|_{\hat{\boldsymbol{x}}(k|k)}, \boldsymbol{H}(k+1) = \frac{\partial \boldsymbol{h}}{\partial \boldsymbol{x}(k+1)}\Big|_{\hat{\boldsymbol{x}}(k+1|k)} \tag{13}$$

$$\boldsymbol{p}(k+1) = \boldsymbol{h}(\hat{\boldsymbol{x}}(k+1|k)) - \frac{\partial \boldsymbol{h}}{\partial \boldsymbol{x}(k+1)}\Big|_{\hat{\boldsymbol{x}}(k+1|k)} \hat{\boldsymbol{x}}(k+1|k) \tag{14}$$

Thus, $\boldsymbol{l}(k+1)$ can be simplified as

$$\boldsymbol{l}(k+1) = \boldsymbol{H}(k+1)\boldsymbol{x}(k+1) + \boldsymbol{p}(k+1) + \boldsymbol{v}(k+1) \tag{15}$$

$\boldsymbol{x}(k+1)$ can be simplified likewise. To deal with IMU drift and noise disturbance, the extended Kalman filter is exerted to the MAV model to fuse the measurement of sonic sensors and the IMU. During the fusion procedure, $\boldsymbol{\Phi}(k+1|k)$ is calculated as

$$\begin{bmatrix} 1 & T_A & 0 & 0 & \frac{1}{2}T_A^2(-a_x(k)\sin\hat{\psi}(k|k) - a_y(k)\cos\hat{\psi}(k|k)) \\ 0 & 1 & 0 & 0 & T_A(-a_x(k)\sin\hat{\psi}(k|k) - a_y(k)\cos\hat{\psi}(k|k)) \\ 0 & 0 & 1 & T_A & \frac{1}{2}T_A^2(a_x(k)\cos\hat{\psi}(k|k) - a_y(k)\sin\hat{\psi}(k|k)) \\ 0 & 0 & 0 & 1 & T_A(a_x(k)\cos\hat{\psi}(k|k) - a_y(k)\sin\hat{\psi}(k|k)) \\ 0 & 0 & 0 & 0 & 1 \end{bmatrix} \tag{16}$$

A concise algorithm is designed as follows to acquire the value of $\boldsymbol{H}(k+1)$.

3.2 Position and Yaw Angle Estimation

The algorithm is derived according to geometric relation between $\boldsymbol{M}_a$ and $\boldsymbol{S}_a$ as shown in Fig. 5.

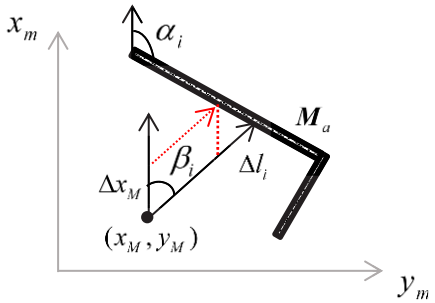

Fig. 5: Geometric relation between $\boldsymbol{M}_a$ and $\boldsymbol{S}_a$ (position estimation)

α_i is the yaw angle of the i^{th} $\boldsymbol{M}_a$, while β_i is the yaw angle of the i^{th} $\boldsymbol{S}_a$. For further analysis, this paper has following assumptions.

Assumption 1: The $\boldsymbol{S}_a$ of the i^{th} sensor between neighbor sampling time remains the same.

Assumption 2: The $\boldsymbol{M}_a$ of the i^{th} sensor between neighbor sampling time remains the same.

Assumption 3: Since the speed of MAV is far less than that of sound, the effect of MAV velocity on measurements of sonic sensors is ignored in this paper.

Note that *Assumption 1* and *Assumption 2* do not always hold and may cause a deviation of the estimation, thus a jump filter is introduced to fix this problem, which will be discussed in section 3.3.

Based on above assumptions, suppose the MAV makes a small increment Δx_M along x_m as shown in Fig. 5, and Δl_i denotes the change of measured value of the i^{th} sensor. It can be derived from the law of sines that

$$\frac{\Delta l_i}{\Delta x_M}=\frac{-\sin(\pi-\alpha_i)}{\sin(\alpha_i-\beta_i)}=\frac{-\sin\alpha_i}{\sin(\alpha_i-\beta_i)} \tag{17}$$

If Δl_i and Δx_M are small enough, the partial derivative of l_i with respect to x_M can be expressed as

$$\begin{aligned}\frac{\partial l_i}{\partial x_M}&=\lim_{\Delta x_M\to 0}\frac{h(x_M+\Delta x_M,y_M,\psi,\mathcal{M},S)-h(x_M,y_M,\psi,\mathcal{M},S)}{\Delta x_M}\\&=\frac{-\sin\alpha_i}{\sin(\alpha_i-\beta_i)}\end{aligned} \tag{18}$$

Therefore, $\frac{\partial l_i}{\partial y_M}$ can be deduced in similar method.

$$\frac{\partial l_i}{\partial y_M}=\frac{\cos\alpha_i}{\sin(\alpha_i-\beta_i)} \tag{19}$$

In the case of yaw angle, a slight change $\Delta\psi$ is exerted on ψ likewise while the estimated value of the i^{th} ultrasonic sensor changes from l_i to $l_i^{'}$ as in Fig. 6.

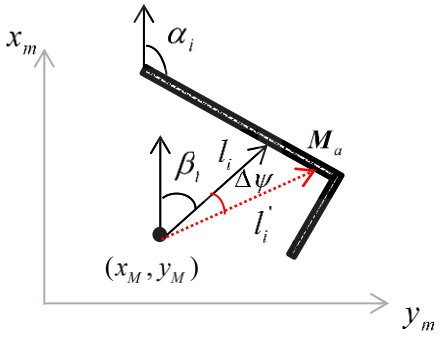

Fig. 6: Geometric relation between $\boldsymbol{M}_a$ and $\boldsymbol{S}_a$ (yaw angle estimation)

The equation between l_i and $l_i^{'}$ can be described as

$$\frac{l_i^{'}}{l_i}=\frac{\sin(\pi-\Delta\psi-(\alpha_i-\beta_i))}{\sin(\alpha_i-\beta_i)}=\frac{\sin(\alpha_i-\beta_i+\Delta\psi)}{\sin(\alpha_i-\beta_i)} \tag{20}$$

Therefore, its partial derivative is formed as

$$\frac{\partial l_i}{\partial\psi}=\lim_{\Delta\psi\to 0}\frac{\Delta l_i}{\Delta\psi}=\lim_{\Delta\psi\to 0}\frac{l_i}{\Delta\psi}\left(\frac{l_i^{'}-l_i}{l_i}\right) \tag{21}$$

Define m_i as $(\alpha_i-\beta_i)$, thus (21) can be diluted as

$$\lim_{\Delta\psi\to 0}\frac{l_i}{\Delta\psi}\left(\frac{\sin(m_i+\Delta\psi)-\sin m_i}{\sin m_i}\right)=\frac{l_i}{\tan(\alpha_i-\beta_i)} \tag{22}$$

According to *Assumption 3*, it can be acquired that

$$\frac{\partial l_i}{\partial v_x}=0,\frac{\partial l_i}{\partial v_y}=0 \tag{23}$$

Consequently, $\boldsymbol{H}(k)$ can be obtained as

$$\boldsymbol{H}(k)=\frac{\partial h_i(k)}{\partial\boldsymbol{x}(k)}=\frac{\partial l_i(k)}{\partial\boldsymbol{x}(k)},i=1,2,3,4 \tag{24}$$

where

$$\begin{cases}\dfrac{\partial l_i(k)}{\partial x_M(k)}=\dfrac{-\sin\alpha_i(k)}{\sin\left(\alpha_i(k)-\beta_i(k)\right)},\dfrac{\partial l_i(k)}{\partial y_M(k)}=\dfrac{\cos\alpha_i(k)}{\sin\left(\alpha_i(k)-\beta_i(k)\right)}\\ \dfrac{\partial l_i(k)}{\partial v_x(k)}=0,\dfrac{\partial l_i(k)}{\partial v_y(k)}=0,\dfrac{\partial l_i(k)}{\partial\psi(k)}=\dfrac{l_i(k)}{\tan(\alpha_i(k)-\beta_i(k))}\end{cases} \tag{25}$$

3.3 Information Fusion by EKF

EKF algorithm is mainly composed of two steps: prediction and estimation. Define the accelerometer sampling interval as T_A, and the sensor sampling interval as T_s. Since T_A and T_s are not the same value, when the ranging data is not updated, MAV yaw angle and location are predicted iteratively by (4)

$$\begin{cases}\hat{\boldsymbol{x}}(k+1\mid k+1)=\hat{\boldsymbol{x}}(k+1\mid k)\\ \boldsymbol{P}(k+1\mid k+1)=\boldsymbol{P}(k+1\mid k)\end{cases} \tag{26}$$

When new data is coming, the prediction is modified by (27), which can be described as

$$\begin{cases}\boldsymbol{l}(k+1)=\boldsymbol{h}(\hat{x}_M(k+1\mid k),\hat{y}_M(k+1\mid k),\hat{\psi}(k),\mathcal{M},S)\\ \boldsymbol{P}(k+1\mid k+1)=\left[\boldsymbol{I}-\boldsymbol{K}(k+1)\cdot\boldsymbol{H}(k+1)\right]\cdot\boldsymbol{P}(k+1\mid k)\\ \boldsymbol{K}(k+1)=\boldsymbol{P}(k+1\mid k+1)\cdot\boldsymbol{H}(k+1)^T\cdot\boldsymbol{R}^{-1}\\ \hat{\boldsymbol{x}}(k+1\mid k+1)=\hat{\boldsymbol{x}}(k+1\mid k)+\boldsymbol{K}_\lambda(k+1)\cdot\left(\boldsymbol{z}(k+1)-\boldsymbol{l}(k+1)\right)\end{cases} \tag{27}$$

where $\boldsymbol{z}(k+1)$ represents the measurement of ultrasonic sensor at sampling time $(k+1)$. Jump filter on gain matrix $\boldsymbol{K}(k)$ is introduced to eliminate mutations due to the switch of $\boldsymbol{M}_a$. The jump filter is formed as

$$\begin{cases}\boldsymbol{K}_\lambda(k)=\boldsymbol{K}(k)\cdot\mathrm{diag}(\lambda_1,\lambda_2,\lambda_3,\lambda_4)\\ \lambda_i=\begin{cases}1 & \left|l_i(k)-z_i(k)\right|\le\varepsilon\\ 0 & \left|l_i(k)-z_i(k)\right|>\varepsilon\end{cases},i=\{1,2,3,4\}\end{cases} \tag{28}$$

where ε is the empirical threshold obtained by experiments, and λ_i is the flag defaulted as 1. The flow of the iterative algorithm is shown in Fig. 7.

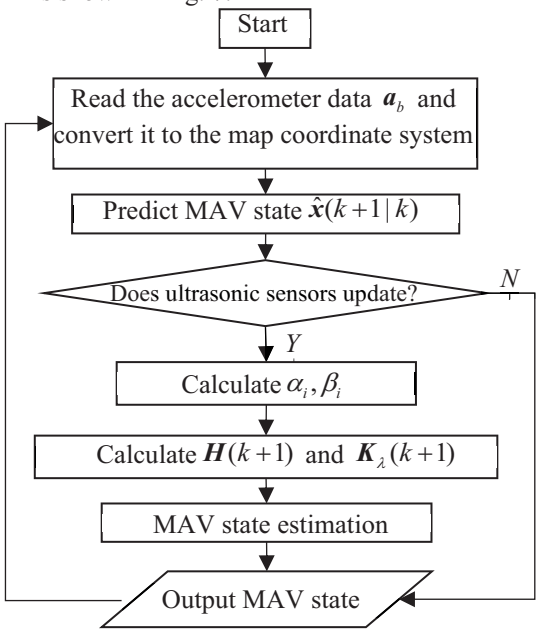

Fig. 7: Flow of EKF

4 Simulation Results

In this paper, flight trajectory of MAV is designed based on polygon map, while control inputs for the MAV are shown in Table 1.

Table 1: Control Inputs of the MAV

Value / Time(s) / Input	0-3.84	3.84-6.24	6.24-7.44
a_x	0.4 m/s^2	0.1 m/s^2	-0.2 m/s^2
a_y	0 m/s^2	-1.8 m/s^2	3.8 m/s^2
ω_z	0 rad/s	0.05 rad/s	-0.05 rad/s

The initial state of the MAV is set as Table 2.

Table 2: Initial State of the MAV

Initial State of the MAV	$x_M(0)$	$y_M(0)$	$v_x(0)$	$v_y(0)$	$\psi(0)$
Value	1 m	1 m	0.05 m/s	0.05 m/s	45°

$\boldsymbol{Q}$ and $\boldsymbol{R}$ are designed as

$$\boldsymbol{Q}=\begin{bmatrix}1&0&0&0&0\\0&0.2&0&0&0\\0&0&1&0&0\\0&0&0&0.2&0\\0&0&0&0&0.2\end{bmatrix},\boldsymbol{R}=\begin{bmatrix}0.02&0&0&0\\0&0.02&0&0\\0&0&0.02&0\\0&0&0&0.02\end{bmatrix} \tag{29}$$

and ε is designed as 0.4. Localization results and the yaw estimation are shown in Fig. 8.

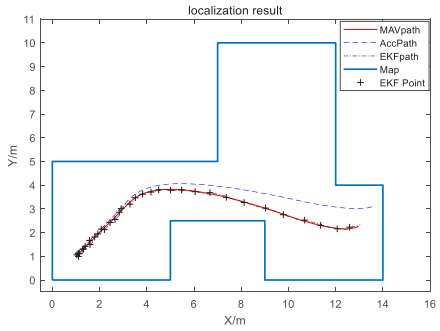

Fig. 8: Localization results

Fig. 8 illustrates the localization results of the EKF information fusion algorithm. MAV actual flight path is shown by the solid line, integral result of IMU is presented by dotted line, and the crosses indicate the estimated points by EKF, thus localized path can be achieved by fitting. In Fig. 9, yaw estimation results are demonstrated.

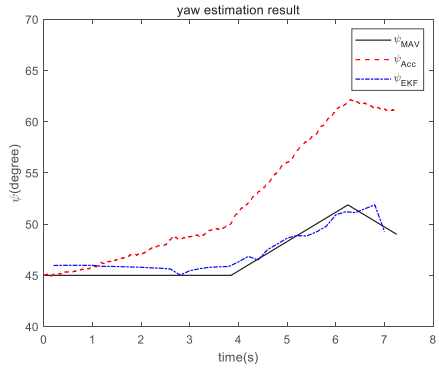

Fig. 9: Yaw angle estimation results

The dotted line is gyroscope integral result on yaw angle, and the dashed line is the yaw estimation of EKF. Solid line shows the actual yaw angle. For quantitative analysis, EKF position estimation error e_{EKF} and IMU integral error e_{Acc} are defined respectively as

$$\begin{cases}e_{EKF}(k)=\left\|\left(x_M(k),y_M(k)\right)^T-\left(\hat{x}_{EKF}(k),\hat{y}_{EKF}(k)\right)^T\right\|_2\\ e_{Acc}(k)=\left\|\left(x_M(k),y_M(k)\right)^T-\left(\hat{x}_{Acc}(k),\hat{y}_{Acc}(k)\right)^T\right\|_2\end{cases} \tag{30}$$

Yaw estimation discrepancies $e_{\psi EKF}, e_{\psi Acc}$ are formed similarly as

$$\begin{cases}e_{\psi EKF}(k)=\left|\psi(k)-\hat{\psi}_{EKF}(k)\right|\\ e_{\psi Acc}(k)=\left|\psi(k)-\hat{\psi}_{Acc}(k)\right|\end{cases} \tag{31}$$

where $(\hat{x}_{EKF}(k),\hat{y}_{EKF}(k))^T,\hat{\psi}_{EKF}(k)$ are the estimated position and yaw angle at sampling time k by EKF, and $(\hat{x}_{Acc}(k),\hat{y}_{Acc}(k))^T,\hat{\psi}_{Acc}(k)$ are the estimated position and yaw angle at sampling time k by IMU. Performance of EKF algorithm is compared to that of IMU as displayed in Fig. 10 and Fig. 11.

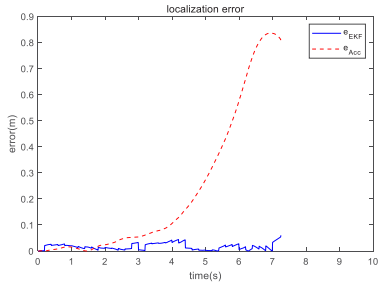

Fig. 10: Positioning error comparison

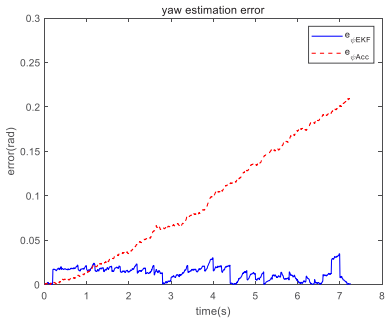

Fig. 11: Yaw estimation error comparison

In Fig. 10 and Fig. 11, the positioning error converges into a neighborhood bounded by 0.1 m, and yaw estimation error is limited in an error band of 0.05rad. When changing the prior map of MAV, the switch of $\boldsymbol{M}_a$ may trigger a jump in the estimation result, whose specific details of neighborhoods of the mutation are shown in Fig. 12. In particular, the jump intersection point is marked as a dotted circle. It shows that the mutation on sonar measurement is led by the switch of $\boldsymbol{r}_a$ and $\boldsymbol{M}_a$.

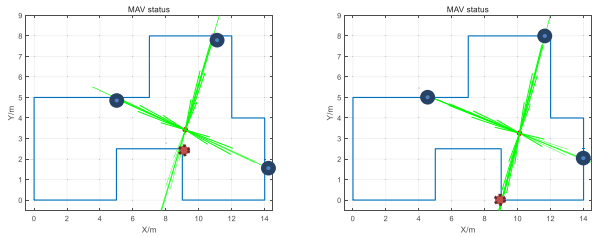

(a) $t = 6$ s (b) $t = 6.2$ s

Fig. 12: Sonar sensors measurement of MAV

Jump filter is introduced under this situation, and results are compared with the original method.

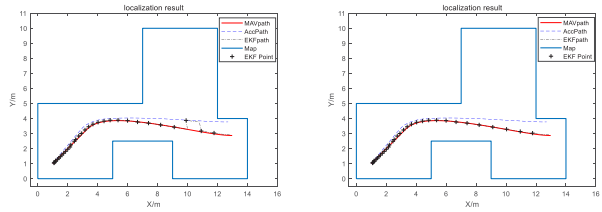

Fig. 13: Positioning comparison by using jump filter

It is shown that the jump filter can remove the mutation and maintain the reliability of EKF according to Fig. 13 and Fig. 14.

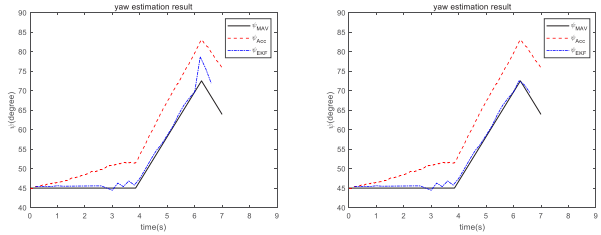

Fig. 14: Yaw estimation comparison by using jump filter

From these figures, it can be seen that the proposed method has improved the performance of MAV yaw angle estimation and localization significantly.

5 Conclusions

A problem of MAV localization and yaw estimation in indoor environment under blocked GPS signals, external magnetic disturbances and noise has been addressed in this paper. A MAV model is established on account of ultrasonic sensors measurement. According to the nonlinearities and implicitness of the model, a low computational cost and fast algorithm based on EKF is developed to estimate MAV position and yaw angle. Moreover, a jump filter is introduced to compensate the mutational effect caused by discontinuity in model function. Simulation results support the validity of the algorithm.

References

[1] L. Yang, X. Feng, J. Zhang, *et al*., Multi-Ray modeling of ultrasonic sensors and application for micro-UAV localization in indoor environments, *Sensors*, 19: 1770, 2019.

[2] Q. Xie, L. Yang, and X. Yang, Micro aerial vehicle indoor localization using prior map and spare sonars, in *Chinese Control Conference*, 2017: 5534–5538.

[3] H. Chen, X. M. Wang, and Y. Li, A survey of autonomous control for UAV, in *International Conference on Artificial Intelligence and Computational Intelligence*, 2009: 267–271.

[4] S. Grzonka, G. Grisetti, and W. Burgard, A fully autonomous indoor quadrotor, *IEEE Transactions on Robotics*, 28(1): 90–100, 2012.

[5] Y. Li, Y. Wang, and D. Wang, Multiple RGB-D sensor-based 3-D reconstruction and localization of indoor environment for mini MAV, *Computers and Electrical Engineering*, 70: 509–524, 2018.

[6] J. Marzat, S. Bertrand, A. Eudes, M. Sanfourche, and J. Moras, Reactive MPC for autonomous MAV navigation in indoor cluttered environments: Flight experiments, in *World Congress of the International-Federation-of-Automatic-Control*, 2017: 15996–16002.

[7] F. M. Jumaah, A. A. Zadain, B. B. Zaidan, A. K. Hamzah, and R. Bahbibi, Decision-making solution based multi-measurement design parameter for optimization of GPS receiver tracking channels in static and dynamic real-time positioning multipath environment, *Measurement*, 118: 83–95, 2018.

[8] P. Lyu, S. Liu, J. Lai, and J. Liu, An analytical fault diagnosis method for yaw estimation of quadrotors, *Control Engineering Practice*, 86: 118–128, 2019.

[9] P. Lyu, Y. Malang, H. Liu *et al.*, Autonomous cyanobacterial harmful algal blooms monitoring using multirotor UAS, *International Journal of Remote Sensing*, 38(8–10): 2818–2843, 2017.

[10] S. Agarwal, S. B. Lazarus, and A. Savvaris, Monocular vision based navigation and localisation in indoor environments, in *IFAC Proceedings Volumes*, 2012: 97–102.

[11] S. Yang, S. A. Scherer, X. Yi, and A. Zell, Multi-camera visual SLAM for autonomous navigation of micro aerial vehicles, *Robotics and Autonomous Systems*, 93: 116–134, 2017.

[12] V. O. Sivaneri and J. N. Gross, UGV-to-UAV cooperative ranging for robust navigation in GNSS-challenged environments, *Aerospace Science and Technology*, 71: 245–255, 2017.

[13] J. Yuan, X. Wang, L. Dong *et al.*, ISILON - An intelligent system for indoor localization and navigation based on RFID and ultrasonic techniques, in *Proceedings of the World Congress on Intelligent Control and Automation*, 2010: 6625–6630.

[14] J. Engel, J. Sturm, and D. Cremers, Camera-based navigation of a low-cost quadrocopter, in *IEEE International Conference on Intelligent Robots and Systems*, 2012: 2815–2821, 2012.

[15] V. Bianchi, P. Ciampolini, and I. De Munari, RSSI-based indoor localization and identification for ZigBee wireless sensor networks in smart homes, *IEEE Transactions on Instrumentation and Measurement*, 68(2): 566–575, 2019.